Crystal Structure Analysis of Phosphatidylcholine−GM2-Activator Product Complexes: Evidence for Hydrolase Activity[†,‡]

Christine S. Wright,*[,⊥] Li-Zhi Mi,[⊥,#] Sangderk Lee,[⊥] and Fraydoon Rastinejad[⊥,§]

Department of Pharmacology, X-ray Crystallography Laboratory, University of Virginia, Charlottesville, Virginia 22908-0735, and Department of Biochemistry and Molecular Genetics, University of Virginia, Charlottesville, Virginia 22908

Received April 12, 2005; Revised Manuscript Received July 28, 2005

ABSTRACT: GM2-activator protein (GM2AP) is a lysosomal lipid transfer protein with important biological roles in ganglioside catabolism, phospholipid metabolism, and T-cell activation. Previous studies of crystal structures of GM2AP complexed with the physiological ligand GM2 and platelet activating factor (PAF) have shown binding at two specific locations within the spacious apolar pocket and an ordering effect of endogenous resident lipids. To investigate the structural basis of phospholipid binding further, GM2AP was cocrystallized with phosphatidylcholine (PC), known to interact with GM2AP. Analysis of three crystal forms revealed binding of single chain lipids and fatty acids only and surprisingly not intact PC. The regions of best defined electron density are consistent with the presence of lyso-PC and oleic acid, which constitute deacylation products of PC. Their acyl tails are in stacking contact with shorter, less well-defined stretches of electron density that may represent resident fatty acids. The GM2AP associated hydrolytic activity that generates lyso-PC was further confirmed by mass spectrometry and enzymatic assays. In addition, we report the structures of (i) mutant Y137S, assessing the role of Tyr^{137} in lipid transfer via the hydrophobic cleft, and (ii) apo-mouse GM2AP, revealing a hydrophobic pocket with a constricted opening. Our structural results provide new insights into the biological functions of GM2AP. The combined effect of hydrolytic and lipid transfer properties has profound implications in cellular signaling.

GM2-activator protein (GM2AP)[1] is one of five well-characterized lysosomal glycosphingolipid activator proteins that play essential roles in the hydrolytic degradation of gangliosides by exo-glycosidases. These enzymatic processes are essential to prevent ganglioside accumulation in neuronal tissue that leads to the fatal condition known as Tay Sachs disease (*1*, *2*). The activator proteins, including four genetically related sulfatide activator proteins (saposins), are characterized by their small molecular size and large hydrophobic pockets for binding long-chain lipids (*3*, *4*). Their best known function is to solubilize specific gangliosides from membranes to be presented to enzyme active sites for removal of the nonreducing terminal sugars.

GM2AP is unique among this family of proteins in that it has high specificity for GM2 (*5*), and its structure is unrelated to that of saposin B (*4*). It acts as a specific cofactor for lysosomal β-hexosaminidase A (HexA), which converts GM2 to GM3 by removal of *N*-acetyl-D-galactosamine (*1*, *5*). Crystal structure analysis revealed a structural fold dominated by a central apolar cup-shaped pocket that consists mostly of β-sheet (*3*) contrasting with the saposins that possess an α-helical fold and function as dimers (*1*, *4*). The spacious pocket is two to three times larger compared with cavities of highly specific lipid-binding proteins (*6*). In addition to their function as enzyme cofactors, these activator proteins have the ability to transfer glyco- and phospholipids between donor and acceptor liposomes in vitro *(5*, *7*, *8*).

In recent years, evidence has emerged for other important biological functions of GM2AP. For instance, involvement of GM2AP in CD1-mediated lipid antigen presentation to T-cells was suggested based on its ability to load and unload specific lipids from CD1d and CD1b molecules in an affinity-based exchange (*9*, *10*). Since both CD1 and GM2AP molecules are localized in the late endosomal compartments, it has been suggested that their interaction could be of vital importance for both immune response and lipid metabolism. Moreover, GM2AP was shown to interact with phospholipids

[†] This research was funded by the National Institute of Health Grant GM 60603.

[‡] Atomic coordinates for GM2AP1-PC, GM2AP2-PC, GM2AP3-PC, Y137S-PC, and mouse-GM2AP are available from the Data Bank with accession codes 2AF9, 2AG2, 2AG4, 2AG9, and 2AGC, respectively.

* Corresponding author. Phone: 434-243-6135; fax: 434-982-3878; e-mail: csw2n@virginia.edu.

[⊥] Department of Pharmacology, X-ray Crystallography Laboratory, University of Virginia.

[§] Department of Biochemistry and Molecular Genetics, University of Virginia.

[#] Present Address: CBR Institute for Medical Research and Department of Pathology, Harvard Medical School, Boston, Massachusetts 02115.

[1] Abbreviations: GM2AP, GM2 activator protein; saposin, sulfatide activator protein; HexA, β-hexoseaminidase A; OMPLA, outer membrane phospholipase A (*Escherichia coli*); PLA2, phospholipase A2; PC, phosphatidylcholine; LPC, lyso-phosphatidylcholine; LPA, lyso-phosphatidic acid; PAF, 1-*O*-alkyl-2-acetyl-*sn*-glycero-3-phosphocholine; PCH, glycero-3-phosphocholine; MYR, myristic acid; LAU, lauric acid; OLA, oleic acid; FA, fatty acid; PED6, *N*-((6-(2,4-dinitrophenyl)-amino)hexanoyl) 2-(4,4-difluoro-5,7-dimethyl-4-bora-3a,4a-diaza-s-indacene-3-pentanoyl)-1-hexadecanoyl-*sn*-glycero-3-phosphoethanolamine, triethylammonium salt; BODIPY-Fl-C5, 4,4-difluoro-5,7-dimethyl-4-bora-3a,4a-diaza-s-indacene-3-pentanoic acid.

10.1021/bi050668w CCC: $30.25
Published on Web 09/21/2005

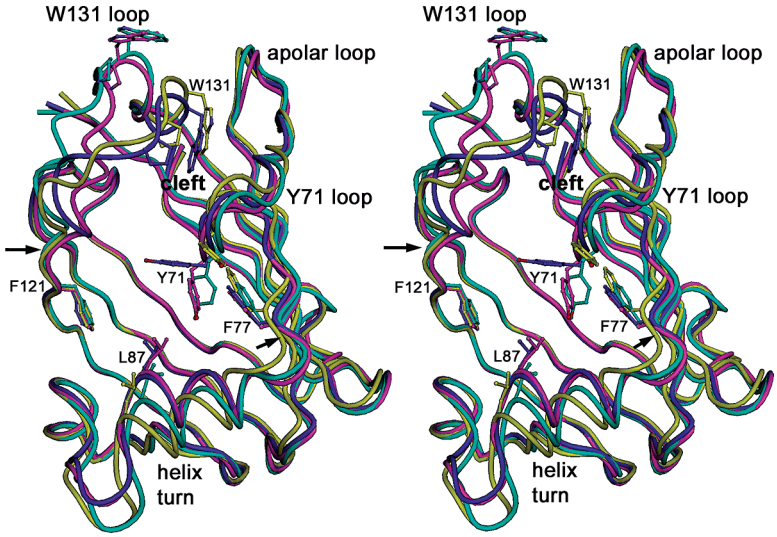

FIGURE 1: Stereoview of the superimposed backbone folds of individual monomers in the three crystal structures GM2AP1-PC, GM2AP2-PC, and GM2AP3-PC. The four loop regions of interest are labeled: W131 loop (Ser^{130}-Thr^{133}), apolar loop (Val^{59}-Trp^{63}), Y71 loop (Thr^{69}-Ile^{72}), and helix−turn (Asp^{85}-Cys^{94}). The sequence numbering convention is for the mature protein of 162 residues. The color code is as follows: cyan, GM2AP1-PC; yellow, monomer B of GM2AP2-PC; magenta, monomer B of GM2AP3-PC; blue, monomer C of GM2AP3-PC. The arrow identifies the starting point of the disordered strand. This figure was prepared with DINO (http://www.cobra.mih.unibas.ch/dino/).

and stimulate the activity of phospholipase D under high salt conditions and in a dose-dependent manner (*11*−*13*).

We have determined a number of crystal structures of GM2AP expressed in *Escherichia coli* with and without added lipid. This work led to identification of regions within the apolar pocket that are used for lipid binding (*6*, *14*). Moreover, comparison of these structures in different crystal forms and crystallographic environments has revealed a high degree of dynamics likely to be a function of lipid association. Flexibility of external loops that decorate the rim of the cavity, a common feature of lipid transfer proteins (*4*, *15*), appears to control the size of the pocket opening and the width of a hydrophobic cleft thought to serve as a lipid transfer channel (*6*). This channel has an open and closed conformation depending on (i) lateral movements of the flexible strand Asp^{125}-Pro^{129} and (ii) the orientation of the mobile Ser^{130}-Thr^{133} reverse turn (termed W131 loop), which has two discrete positions (*6*) (see Figure 1).

In those structures in which the cleft is open, bound lipid is observed within the hydrophobic cleft (site I) as well as deep inside the pocket (site II) (*14*). Analysis of these structures revealed that the headgroups of bound GM2 and phospholipids occupy different locations. The GM2 tetrasaccharide moiety was found to be disordered, as it is exposed on the protein surface (*6*). It was modeled in a region close to the single alpha-helix. Phospholipids bind in two positions with their headgroups partly bound in hydrophobic environments. In the case of bound platelet activating factor (PAF), one molecule binds near the side chain of Ser^{141} inside the pocket, and the second molecule interacts with the side chain of Tyr^{137} at the entrance of the cleft (*14*). The alkyl chains are positioned inside the pocket and not near the flexible peptide strand (Asp^{125}-Leu^{128}), as suggested by Wendeler et al. (*16*) based on photoaffinity labeling studies.

Here, we describe the structures of three new crystal complexes of GM2AP, prepared in the presence of 1,2-dioleoyl-*sn*-glycero-3-phosphocholine (PC). The ability of GM2AP to interact with PC has been suggested in several studies previously but was never structurally characterized (*5*, *12*, *13*). PC is the most common phospholipid in eukaryotes. Because of its low aqueous solubility, it requires transport by specific transfer proteins, such as human PC transfer protein whose crystal structure is known (*15*). Importantly, none of the three crystal structures analyzed show bound PC inside the hydrophobic pocket. The electron density is consistent only with bound single chain lipids, suggesting that PC has been hydrolyzed. Crystallographic and solution data are presented confirming that hydrolytic activity is associated with GM2AP. Two additional structures were investigated: (i) the Y137S-PC mutant, testing the involvement of Tyr^{137} in phospholipid headgroup binding and stabilization of the mobile W131 loop, and (ii) apo-mouse GM2AP to better understand its unique binding properties toward GM2 and HexA and its milder Tay Sachs symptoms (*17*, *18*).

EXPERIMENTAL METHODS

Human GM2AP PC Complexes. (a) Crystallization and Data Collection. Human wild-type GM2AP and the Y137S mutant were expressed in *E. coli* using a His-tag expression vector and purified as described previously (*6*). 18:1 PC was purchased from Avanti Polar Lipids Inc. The following protocol was used for the cocrystallization experiments: Fifteen microliters of 12.7 mM PC (10 mg/mL in chloroform) was evaporated on a glass slide. The dry residue was solubilized in a small volume of ethanol and subsequently combined with 150 μL of the 0.3 mM protein solution (5.4 mg/mL) prepared in 25 mM ammonium acetate buffer (pH 5.0). The molar excess of PC over protein in the reaction mixture was 3:1. After 3 h of incubation at room temperature, the mixture was applied to a 0.8 × 15 cm S-200 Sephacryl column, equilibrated with 25 mM ammonium acetate buffer (pH 6), to remove unbound micellar phospholipid material. The eluted fractions were pooled and concentrated to 10 mg/mL in a Beckmann GS-15R centrifuge for crystallization. To verify the presence of lipid, a 30 μL sample was extracted

Table 1: Crystal Data for PC Complexes

structure	space group	pH[a]	#[b]	cell dimensions					
				a	*b*	*c*	α	*β*	*γ*
GM2AP1-PC	$P2_12_12_1$	5.6	1	39.10	41.98	114.21	90.00	90.00	90.00
GM2AP2-PC	$P2_1$	7.3	2	41.50	64.09	80.99	90.00	92.81	90.00
GM2AP3-PC	$P2_12_12_1$	7.6	3	63.53	86.19	120.48	90.00	90.00	90.00
Y137S-PC	P1	7.9	2	41.49	48.39	55.59	76.16	87.70	87.54

[a] Buffer consists of 0.1 M Hepes, 10% 1-propanol, 22−25% PEG 4000. [b] Number of monomers in the asymmetric unit.

Table 2: Refinement Statistics

	GM2AP3-PC	GM2AP2-PC	GM2AP1-PC	Y137S-PC	mouse
		Data Collection			
wavelength (Å)	1.0000	0.97943	0.97943	0.92015	1.54051
d_{min} (Å)	2.00	1.80	1.95	2.0	2.5
unique reflections	45,405	37,989	13,638	18,933	7121
$\langle I/\sigma(I)\rangle$[a]	26.0(7.7)	14.0(4.0)	18.0(2.5)	10.0(1.7)	10.0(2.5)
completeness (%)[a]	99.9(99.9)	95.4(90.3)	95.0(99.9)	66.6(26.0)	94.5(94.2)
mean redundancy[a]	5.5(5.3)	3.4(3.3)	6.4(6.3)	1.8(1.1)	1.7(1.8)
R_{merge} (%)[b]	6.9(19.5)	4.3(10.9)	4.0(6.4)	8.2(29.1)	6.1(33.3)
		Structure Refinement			
resolution range (Å)	20−2.0	20−1.8	20−2.0	20−2.2	15−2.5
reflections used	45,347	37,646	12,607	16,412	6,869
no. monomers per AU	3	2	1	2	1
no. protein atoms	3714	2508	1241	2504	1243
no. waters	594	641	115	252	66
no. buffer atoms	70	48	8	52	0
no. ions	3				
no. ligand atoms	254	110	64	16	44
R_{cryst} (%)[c]	18.80	18.83	22.03	24.90	21.79
R_{free} (%)	23.10	22.38	27.39	32.75	28.26
rms deviations angles (°)	1.53	1.48	1.49	1.57	1.73
rms deviations bonds (Å)	0.01	0.009	0.010	0.010	0.012
Luzzati coordinate error (Å)	0.21	0.19	0.25	0.35	0.29
average atomic B-factor (Å^2)	29.7	26.7	32.9	38.93	52.1
protein	24.9	21.5	31.3	35.04	51.1
water	36.5	37.6	37.25	53.91	64.8
lipid	67.6	61.6	57.8	45.69	62.3
buffer[d]	55.7	61.8	63.0	45.50	63.0

[a] Values in parentheses are for the highest resolution shell. [b] $R_{merge} = \sum\sum|I_i - \langle I\rangle|/\sum\langle I\rangle$, where I_i refers to the intensity measurement of a given equivalent reflection *hkl*. [c] $R_{cryst} = \sum||F_o| - |F_c||/\sum|F_o|$. [d] Buffer atoms are from bound Hepes and 2-propanol molecules.

with chloroform/methanol (2:1) and analyzed by mass spectrometry. Two major peaks were observed at masses of 522.3 for lyso-PC (lyso-1-oleolyl-*sn*-glycero-3-phosphocholine) and 786.5 for PC, indicating cleavage at the *sn*-2 acyl bond. Purity of the PC reagent was confirmed by mass spectrometry analysis, which showed a single mass at 786.5.

Crystallization trials yielded three types of well-ordered crystals that diffracted beyond 2 Å resolution (see Table 1). These crystals grew within one week by the hanging drop vapor diffusion technique at 5 °C from a buffer solution containing 21−25% (w/v) poly(ethylene glycol) (PEG) 4000, 10% (v/v) 2-propanol and 0.1M Hepes buffer at pH values of 5.6, 7.3, and 7.6. Droplets prepared by mixing 2 μL of the protein solution with 2 μL of reservoir buffer solution were equilibrated over 0.5 mL of reservoir buffer. Crystals grown from 25% PEG4000 at pH 5.6 and 7.6 were of similar morphology as those of the apo protein (*3*, *19*). A highly ordered monoclinic crystal form ($P2_1$) was obtained from 21% PEG4000 at pH 7.3, diffracting to 1.6 Å resolution.

The PC complex of the Y137S mutant was prepared similarly and crystallized using a 7.0 mg/mL protein solution and a 22% PEG4000 reservoir buffer (pH 7.9). The crystal morphology consisted of thin plates that tended to form multiple stacks. These crystals belong to space group *P*1 and possess a small cell of two independent monomers (see Table 1). The intensity data measured to 2 Å resolution scaled with a relatively high scaling R-factor (8−10%). This is believed to be due to large absorption effects reflected in the wide range of of scale factors (0.26−1.0) and mosaicities (0.45 to 1.26) between images.

For data collection crystals were mounted by flash-freezing. During mounting, the crystallization droplet was covered with parafin oil to prevent evaporation of 2-propanol. Data collection was carried out at beamlines IMCA-CAT and SERCAT (APS Argonne National Laboratory). X-ray data were collected to resolution limits and reduced with HKL2000 (*20*). Final statistics are summarized in Table 2.

(b) Structure Determination and Refinement. The structures of the new crystal forms, GM2AP2-PC and Y137S-PC, were solved by molecular replacement using the program MOLREP (*21*, *22*). Monomer B of the human apo structure (1PU5) served as search model for the rotational and translational searches of GM2AP2-PC. In the case of Y137S-PC, the GM2AP2-PC dimer provided an excellent search model. The initial models were examined with "O" (*23*) and submitted to rigid body refinement and minimization, using CNS (*24*), followed by model inspection. Structure refinement of all four structures was carried out with the program

suite CNS (Table 2). The structure of Y173S-PC was refined at 2.2 Å resolution because of the lack of completeness at 2.0 Å resolution (67%). Water, solvent, and lipid molecules were gradually added in the refinement process. Bound lipid and fatty acids were located from "composite omit" maps after three cycles of structure refinement at 2.5 Å resolution and characterized according to the size and shape of the available electron density. The final models adhere to proper stereochemistry showing 100% of the amino acid residues in allowed regions of the Ramachandran plot analyzed with PROCHECK (*21*). Model coordinates for LPC, OLA, MYR, and LAU were obtained from the HICUP server (*25*). Electron density maps were computed and structure analysis carried out with the program suite CCP4 (*21*). Modeling was performed with the graphics program O (*23*).

Mouse-GM2AP. Wild-type mouse-GM2AP was prepared by the same protocol as human GM2AP (*17*, *19*).

The protein (8 mg/mL in 0.02 M phosphate buffer, pH 6.5) was crystallized by the hanging drop vapor diffusion method from a crystallization reservoir (0.5 mL) containing 22.5% PEG 4000, 0.1 M sodium acetate buffer, pH 5.6, and 0.2 M ammonium acetate. Droplets of 6 μL of protein were mixed with 4 μL reservoir buffer and equilibrated over 0.5 mL reservoir buffer. Large rhombohedral crystals grew at room temperature within two weeks. These crystals belong to space group $P2_12_12_1$ with cell dimensions $a = 42.98$ Å, $b = 51.27$ Å, and $c = 92.3$ Å and one monomer per asymmetric unit. X-ray intensity data were measured at room temperature on an in-house Rigaku R-AXIS IIC image plate detector mounted on a Rigaku rotating anode X-ray generator and were reduced with HKL2000 (*20*). The data extended to 2.5 Å resolution and scaled with an R_m of 6.1% (see Table 2). Using monomer A of human GM2AP (1G13) as search model, the structure was determined by molecular replacement and subsequently refined with CNS (*24*) (see Table 2).

Fluorimetric Phospholipase A2 Activity Assay. Human GM2AP was prepared using a bacterial expression system as described previously (*6*). Purified protein solutions were diluted with 25 mM ammonium acetate buffer (pH 6.0) such that 1 μg was contained in the assay mixture of 100 μL (protein concentration around 0.56 μM). To selectively measure hydrolysis at the *sn*-2 ester bond, the bifunctional fluorescent substrate PED6 (*N*-(6-(2,4-dinitrophenyl) amine)-hexanoyl 2-(4,4-difluoro-5,7-dimethyl-4-bora-3a,4a-diaza-s-indacene-3-pentanoyl)-1-hexadecanoyl-*sn*-glycero-3-phosphoethanolamine triethylammonium salt) was used (purchased from Molecular Probes Inc., Eugene, OR). A 1.0 mM stock solution of PED6, solubilized in ethanol, was prepared and serially diluted with the assay buffer yielding a concentration range of 50−0.05 μM. The solution was incubated for 30 min at room temperature. Fluorescence intensity measurements were made at excitation and emission maxima of 475 and 525 nm, respectively, using a FlexStation (Molecular Devices). The values were compared to a standard curve prepared with the fluorescent product fatty acid BODIPY-Fl-C5 (4,4-difluoro-5,7-dimethyl-4-bora-3a,-4a-diaza-s-indacene-3-pentanoic acid).

Time Study of LPC Production in the PC/GM2AP Reaction Mixture. The enzyme autotaxin, a mammalian lyso-phospholipase D (lyso-PLD), was used to detect the presence of LPC in GM2AP/PC reaction mixtures. Cleavage occurs at the phosphodiester bond with the release of choline, detected colorimetrically by use of an enzyme cocktail containing choline oxidase and horseradish peroxidase (*26*). The assay conditions were as follows: A 60 μL reaction mixture containing GM2AP (2.5 mg/mL) dissolved in 25 mM ammonium acetate (pH 6.0), and 1 mM 18:1 PC solubilized in ethanol was incubated at room temperature for various time periods.

Samples of 9 μL were removed at 2, 4, 8, 22, 33, and 50 h of incubation. As a control, the same reaction mixture was prepared in the absence of GM2AP, as well as in the presence of 2% β-octylglucoside and 0.1% Triton X-100. The 9 μL aliquots were diluted to 100 μL by addition of a pH 8.0 buffer composed of 0.1 M Tris-HCl, 0.15 M NaCl, 5 mM $MgCl_2$, 0.05% Triton X-100. This solution was incubated for 1 h at 37 °C with 1 μg of autotaxin prepared as described previously (*27*). Subsequently, an equal volume of enzyme cocktail, containing 50 mM Tris-HCl, 5 mM $MgCl_2$, 2.7 mM *N*-ethyl-*N*-(2-hydroxy-3-sulfopropyl)-*m*-toluidine (TOOS), 4.5 mM 4-aminoantipyrine, 47.7 u/mL horseradish peroxidase, 18 u/mL choline oxidase, was added, and the mixture was incubated for 15 min at 37 °C. The amount of choline release was calculated by measuring the absorbance at 550 nm using a standard curve for choline.

RESULTS

1. Structure Refinement of Different Crystal Forms. Tables 1 and 2 summarize the crystallization data and refinement statistics for the five structures presented here. The low and high pH orthorhombic crystal forms, GM2AP1-PC and GM2AP3-PC, correspond to those of apo-GM2AP (*3*, *6*, *19*), with one and three monomers per asymmetric unit, respectively. GM2AP2-PC and Y137S-PC represent new crystal forms of lower symmetry ($P2_1$ and $P1$). Both structures crystallized as thin plates and contain an identical noncrystallographic dimer in the asymmetric unit. GM2AP2-PC is the best refined structure at 1.8 Å resolution, including a large number of water molecules (Table 2). The structure of the Y137S mutant is of lower quality, retaining a high value of R_{free} (32.75%) despite extensive efforts of refinement and model building (see Table 2). This is partly due to poor crystal scaling and lack of completeness of the 2.2 Å resolution data (77%).

GM2AP1-PC represents a more highly refined low pH structure of GM2AP at 2 Å resolution compared with the corresponding 2.5 Å apo structure (*6*). It includes a larger number of waters and four well-defined fatty acid molecules (see Table 2). Mouse apo-GM2AP, which has 73.5% sequence identity with the human protein, was also crystallized in space group $P2_12_12_1$ under low pH conditions (pH 5.6). This crystal form differs from that of human GM2AP1 both in cell size and molecular packing.

Table 3 summarizes the types of lipid and fatty acid molecules refined in four of the structures reported here. The high values of their atomic B-factors (50−70 Å^2) (Table 2) are typical for thermally disordered loosely associated lipids. The combined information from the structures reported here and from previously determined ligand complexes (*6*, *14*) has allowed us to identify preferred binding regions within the spacious hydrophobic pocket. All binding regions identified contain at least one aromatic side chain (Tyr^{137}, Tyr^{71},

Table 3: Tentative Assignment of Ligand Type in Different Structures

structure	site I (hydrophobic cleft)	site II (pocket)	other
GM2AP1-PC	MYR, LAU	OLA	LAU
GM2AP2-PC-A[a]		LPC	OLA
GM2AP2-PC-B[a]		PLC	OLA
GM2AP3-PC-A[a]	LPC	LPC	
GM2AP3-PC-B[a]	PCH, OLA, LAU	LPC	MYR
GM2AP3-PC-C[a]		LPC	OLA, MYR, PCH
Y137S-PC-A[a]		none	
Y137S-PC-B[a]			MYR

[a] Monomer type. MYR, myristic acid; LAU, lauric acid; OLA, oleic acid; LPC, lyso-phosphatidylcholine (1-oleoyl-2-hydroxy-*sn*-glycero-3-phosphocholine); PCH, 1,2-hydroxy-*sn*-glycero-3-phosphocholine.

Tyr^{114}, Phe^{77}, Phe^{80}, Phe^{109}, Phe^{121}), as discussed below. Figure 2 illustrates the strong degree of overlap of bound lipid in the three PC complexes, although their identity at specific locations varies among the structures.

2. Binding Locations for lyso-PC. LPC was found to occupy the same two sites within the hydrophobic pocket as observed for PAF in the GM2AP−PAF complex (*14*). Its identity was unambiguously established through the characteristic electron density features for its phosphocholine headgroup and location near polar side chains. The most highly and consistently occupied region of the binding pocket in both the open and the closed structures is that of binding site II. Here, LPC is deeply immersed inside the pocket. It is represented by strong electron density (Figure 3a) with its headgroup bound in the vicinity of the side chains of Ser^{141}, Phe^{80}, Phe^{109}, and Tyr^{114}. However, its bound conformation as well as its position differs in the structures of GM2AP2-PC and GM2AP3-PC. The headgroups are shifted by several angstroms with respect to one another and the alkyl chains extend along different directions. In GM2AP2-PC the acyl tail is nestled against the α-helix with its distal end extending away from the protein surface, while in GM2AP3-PC it remains in van der Waals' contact with other alkyl chains within the pocket (see Figures 3b and 4a).

Binding site I is occupied in those structures in which the W131 mobile loop is flipped out and the hydrophobic cleft is open (monomers A and B of GM2AP3-PC, and GM2AP1-PC) (Figure 4a). Since this cleft is believed to serve as lipid transfer channel, occupancy may be transitional (*6*). As described for the PAF complex (*14*), where the open conformation is seen in all three monomers (A,B,C), the positively charged phosphocholine headgroup is immobilized through stacking contact with Tyr^{137} and several nonpolar side chains on either side of the cleft (Leu^{55}, Ile^{66}, Ile^{72}, Leu^{126}, Leu^{128}, Leu^{132}) (see Figure 4b). It is interesting to note that a nonpolar environment is also observed for the phosphocholine headgroup in the PC complex of the human PC transfer protein (*15*). The available electron density for LPC is continuous only in monomer A. In monomer B, a gap at the *sn*-1 acyl bond suggests either conformational disorder or enzymatic cleavage of the oleate group (Figure 4b). It is worth noting that a gap in the electron density along the acyl tail, consistently observed for LPC and OLA, coincides with the unsaturated bond C9═C10. Since it is well-known that unsaturated lipids are susceptible to oxidation (*28*), this may reflect limited cleavage of some of the oleate chains.

3. Fatty Acid Association. The binding pockets of each of the five structures examined contain extended stretches of electron density that could be modeled as alkyl chains 12−18 carbons in length (Table 3). Their presence may derive from two sources: (i) cleavage of the acyl tail of PC, as evidenced by the presence of bound OLA in GM2AP1-PC, GM2AP2-PC, and GM2AP3-PC (see Table 3), and (ii) fatty acids that were trapped during refolding and solubilization of the protein from inclusion bodies. While their identity may differ at specific binding locations, they were typically found to be associated with acyl chains of LPC or other fatty acids. The longest stretches of electron density were modeled as OLA, although there is no clear evidence that it derives from hydrolysis of PC. OLA is particularly well defined in binding site II of GM2AP1-PC (Figure 4a). This low pH structure, with a wide open binding pocket, contains fatty acids only and no LPC (Table 3).

In GM2AP2-PC, a shorter stretch of electron density that runs parallel to the LPC acyl tail was modeled as OLA (Figure 3b). Although the available electron density extends only up to carbon-12, proximity of its carboxylate group to the glycerol *sn*-2 hydroxyl of LPC and the fact that this structure is devoid of ordered resident fatty acids support this assignment.

The presence of OLA was also unambiguously established at site I in monomers B and C of GM2AP3-PC (figures 3b, 4b). As shown in Figure 4b, three fatty acids are in stacking contact in binding site I of monomer B. They are in van der Waals' contact with the glycerol-3-phosphocholine group (PCH) (3.2−4.0 Å), although an electron density connection is lacking. Such ordering of lipid tails has been observed previously in the structures of liver fatty acid binding protein and lipovitellin (*29*, *30*). A third binding location exists in the vicinity of the Y71 loop where ligand binding (MYR and PCH) appears to have an ordering effect on the flexible side chain of Tyr^{71}. PCH binds in stacking contact with the aromatic side chain of Tyr^{71} in monomer C. A similar contact is observed in site I of monomer B where the phosphocholine moiety of LPC interacts with the side chain of Tyr^{137} (see Figures 3b and 4b).

4. Structure Comparisons. The α-carbon backbone folds of GM2AP1-PC, GM2AP2-PC and GM2AP3-PC are compared in Figure 1. They are examples of both the open and the closed conformations of the molecule. Pairwise structural superpositions show average discrepancies > 1.0 Å except in those cases in which multiple copies within the asymmetric unit are compared (see Table 4). The largest differences are confined to three flexible loop regions: (1) the flexible peptide Pro^{124}-Ser^{130} followed by the mobile W131 loop (Ser^{130}-Thr^{133}), controlling the entrance to the cleft; (2) the Y71 reverse turn (Thr^{69}-Ile^{72}) and (3) the helix−turn region (residues Phe^{80}-Cys^{94}). Movements in these regions affect the diameter of the pocket opening. Mobility of the first two regions has previously been described for the three independent monomers of the apo structure (*3*, *6*). As shown in Figure 1, the lateral shifts of peptide Asp^{125}-Leu^{128} occur in both the open and the closed structures. For instance, this strand is folded back by several angstroms in GM2AP1-PC, which has a wide open cleft, and in the closed structure of monomer C of GM2AP3-PC. Shifts in the Y71 loop are small, although the side chains of Asp^{70} and Tyr^{71} are very flexible.

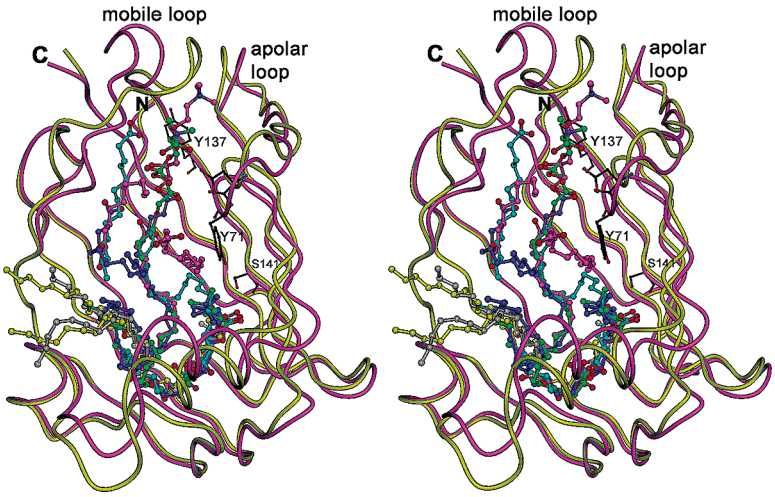

FIGURE 2: Structural alignment of bound ligands inside the apolar pocket of all independent monomers in the three PC complexes. The backbone folds displayed are for monomer B of GM2AP2-PC (yellow) and monomer B of GM2AP3-PC (magenta), as examples of a closed and open structure. Color code for bound lipid is as specified in Figure 1. Bound lipid in monomers A of GM2AP2-PC and GM2AP3-PC (not shown in Figure 1) are colored gray and green, respectively. Figure was prepared with DINO.

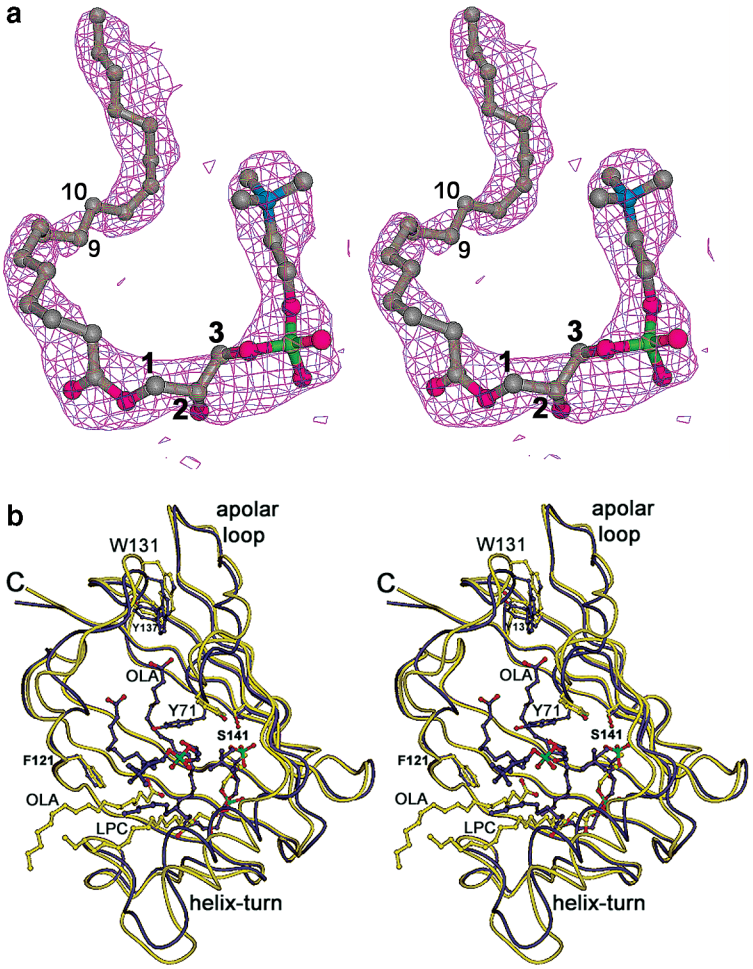

FIGURE 3: Ligand binding at site II. (a) LPC superimposed onto the $2F_o - F_c$ electron density map (contoured at 1σ) in monomer B of GM2AP3-PC. The carbon atoms of the glycerol moiety are labeled 1, 2, 3. The unsaturated labile bond of the oleate acyl chain is located at position C9═C10, showing weak electron density. (b) Comparison of bound ligand in the two "closed" structures of GM2AP2-PC (monomer B) and GM2AP3-PC (monomer C).). The ligands are labeled LPC for lyso-phosphatidylcholine and OLA for oleic acid. The coloring convention is as specified in Figure 1. Figure was prepared with DINO.

The previously unobserved conformational change in the helix−turn region is seen in the structures of GM2AP2-PC, Y137S-PC, and GM2AP1-PC. The α-helix takes up a new position as a result of an outward rotation of its helical axis by 30−40° and strand separation of β-strands 4 and 5 due to loss of the outer hydrogen bond between Leu[49] and Phe[80].

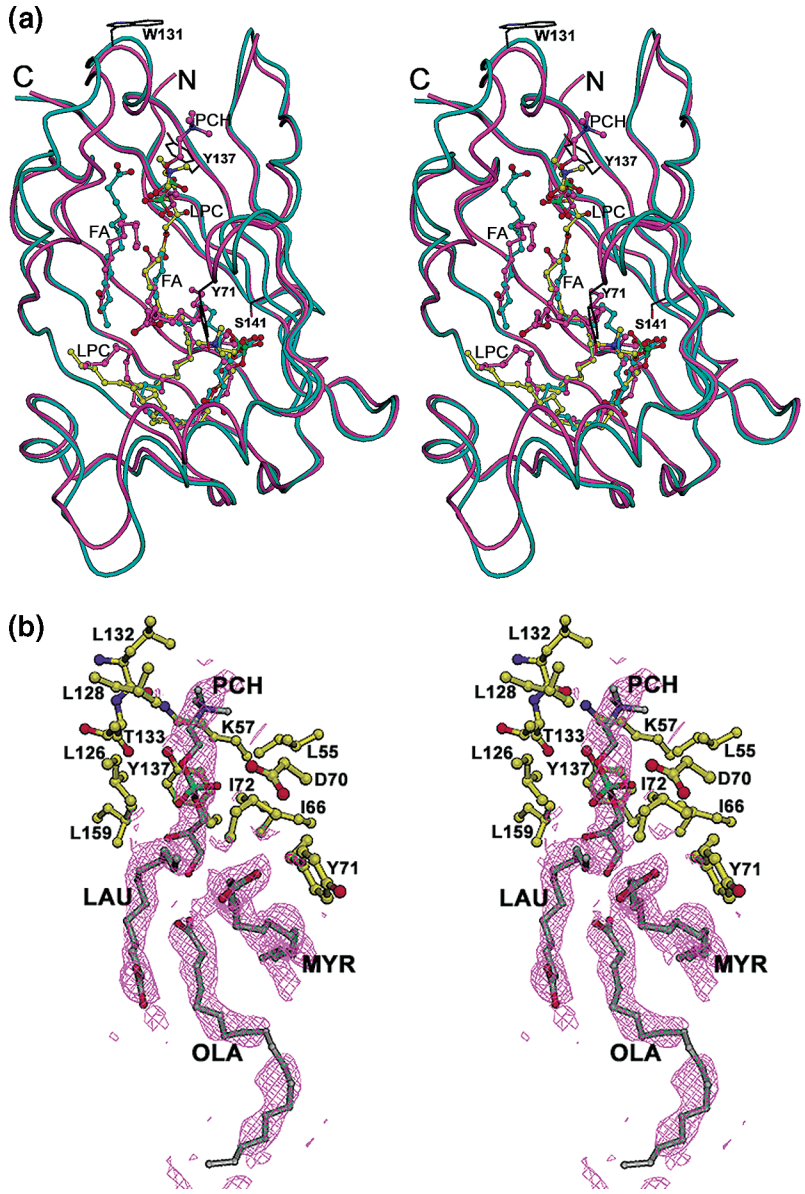

FIGURE 4: Stereoview of lipid bound at sites I and II in structures that possess the "open" conformations of the hydrophobic cleft. (a) Bound lipid is shown superimposed for GM2AP1-PC (cyan), GM2AP3-PC (monomer B) (magenta), and GM2AP3-PC (monomer A) (yellow). The backbone folds correspond to those of GM2AP1-PC and GM2AP3-PC (monomer B) and selected amino acid side chains belong to GM2AP3-PC (monomer B). The labels PCH and FA refer to glycero-3-phosphocholine and fatty acid, respectively. The N- and C-termini are labeled N and C. (b) Close-packed environment of the PCH group in site I of monomer B (GM2AP3-PC). The $2F_o - F_c$ electron density map, contoured at 0.9σ, illustrates a break at the *sn*-1 glycerol acyl bond. The separate electron density fragments are modeled as OLA, MYR, and LAU. Figure was prepared with DINO.

Table 4: Superposition of Refined Structures

structure	type	all atoms[a]	C_a atoms[a]
open monomers			
GM2AP3−PC	A/B monomers	1.16	0.72
GM2AP1/GM2AP3−PC	A monomers	1.52	1.20
closed monomers			
GM2AP2−PC	A/B monomers	0.53	0.21
Y137S−PC	A/B monomers	1.06	0.39
GM2AP2−PC/Y137S−PC	AB dimers	1.26	0.89
GM2AP2/GM2AP3−PC	B/C monomers	1.67	1.37

[a] Values were calculated with the program LSQKAB (*21*) and represent rms Δ in Å.

In view of nonpolar contacts of several of the helix side chains with the LPC acyl tail, this conformational change may be due to lipid binding.

5. Importance of Tyr[137] for Ligand Binding. The importance of Tyr^{137} for phospholipid binding was investigated by introducing a serine mutation. Tyr^{137} is located in a strategic position at the entrance of the cleft (Figure 2), providing stabilizing interactions for both the open and the closed conformations of the mobile W131 loop and for the phospholipid headgroup in GM2AP3-PC and GM2AP-PAF (*14*). Although the crystals of Y137S obtained after incubation with PC were not as highly ordered as those of wild-type GM2AP, structure analysis at 2.2 Å resolution clearly showed significant rearrangements in the region of the disordered strand and at the W131 loop (Ser^{130}-Thr^{134}). As illustrated in Figure 5b, the W131 loop has adopted a new conformation as a result of the serine mutation. Both Trp^{131} and Lys^{57} take up new positions due to loss of their van der

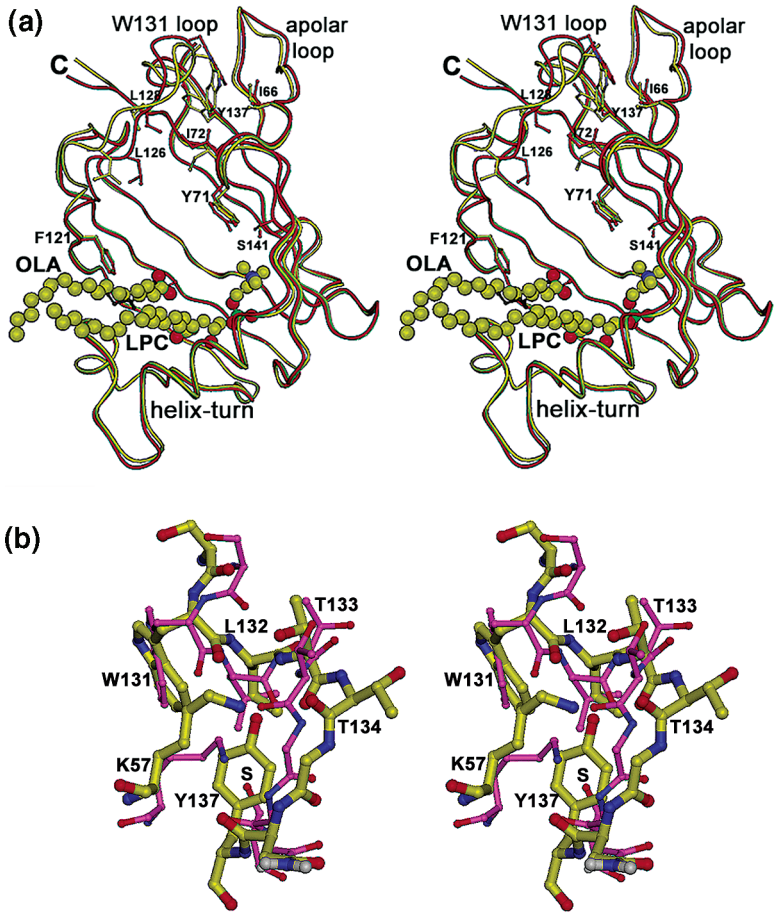

FIGURE 5: Stereoscopic illustration of the structural changes between mutant Y137S-PC and the corresponding "closed" structure of GM2AP2-PC. (a) The backbone folds of monomer B are shown in yellow and red for GM2AP2-PC and Y137S-PC, respectively. LPC and OLA at site II of GM2AP2-PC are represented as van der Waals' spheres. The single fatty acid molecule present in Y137S-PC is depicted in black as "ball-and-stick", coinciding with the position of OLA. (b) Close-up view of the conformational differences in the mobile W131 loop. The mutant structure is shown in red. The serine side chain is designated by "S". Figure was prepared with DINO.

Waals' contact with the aromatic ring of Tyr^{137}. The indole ring of Trp^{131} is in a more exposed position relative to that observed in GM2AP2-PC and Lys^{57} forms new hydrogen bonds with the carbonyl groups of Thr^{134} and Glu^{58}. The side chains of Thr^{133} and Thr^{134} have shifted into new positions due to changes in the dihedral angles of the peptide region Leu^{132}-Thr^{134}. The flexible peptide Asp^{125}-Pro^{129} moved inward making contact across the cleft with the side chain of Ile^{72} (see Figure 5a).

Electron density features inside the pocket are patchy and were modeled as eight 2-propanol molecules in monomer A. Neither PC nor LPC are seen bound in binding position II near Ser^{141} and at the Y71 loop, where the side chains of Asp^{70} and Tyr^{71} are partly disordered. Only one stretch of electron density indicated fatty acid binding. It is located in monomer B and coincides with the general position of OLA in GM2AP2-PC (see Figure 5a).

6. Mouse-GM2AP: Example of a Low pH Closed Structure. The most interesting feature of the mouse-GM2AP structure is its overall compact fold and constricted cavity opening (10 Å diameter) relative to the closed crystal structures of human GM2AP3-PC and GM2AP2-PC (Figure 6). Sequence comparisons show that the flexible chain segment Asp^{125}-Thr^{134} and many of the hydrophobic residues inside the pocket are completely conserved. Moreover, the apolar character of the exposed reverse turn Val^{59}-Trp^{63}, thought to interact with membrane bilayers (*6*), is further enhanced in mouse-GM2AP by replacement of Leu^{62} with Phe. The Y71 reverse turn has a series of mutations (D70E, Y71Q, and I72L), which probably accounts for the specificity differences between human and mouse GM2AP for the GM2 carbohydrate moiety (*6*, *18*).

Interpretation of the electron density map revealed fragmented electron density inside the pocket in similar position as found in the structure of human GM2AP3-PC (monomer C). This density was tentatively modeled as three fatty acid molecules with alkyl chains 12−14 carbons in length (MYR, LAU) (see Figure 6). As also observed in the structures of human apo-GM2AP (*3*) and SapB (*4*), this lipid material co-purified from the inclusion bodies and may be required for structural stability. When the three fatty acid molecules were oriented with their carboxylate groups at the high-density end, favorable interactions with aromatic side chains and hydroxyl groups (Tyr^{87}, Phe^{62}, Ser^{141}) became possible (Figure 6).

7. Analysis of Phospholipase A Activity. LPC is generated through cleavage of the *sn*-2 acyl bond of PC. The crystallographic evidence for LPC suggests that the type of enzymatic activity associated with GM2AP is reminiscent of that of phospholipase A2 (PLA2). Two independent assays were performed to analyze this observed activity in solution. First, LPC production was monitored enzymatically over a

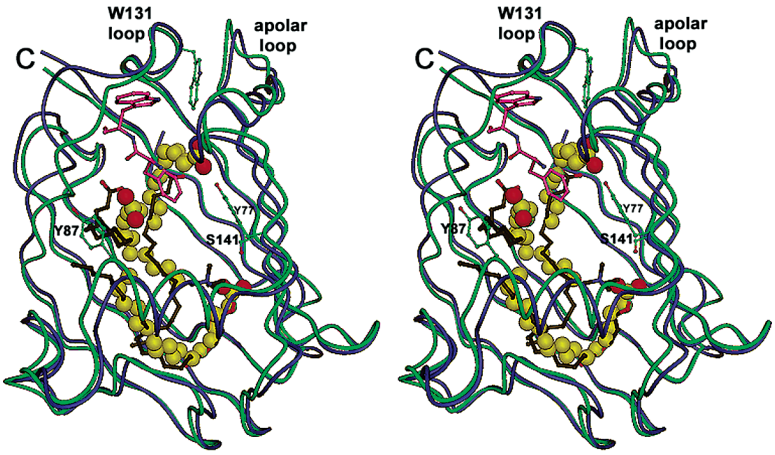

FIGURE 6: Stereoview comparing the polypeptide folds of mouse GM2AP (green) with monomer C of human GM2AP3-PC (navy). The three fatty acid molecules in the mouse structure are depicted as yellow spheres. The ligands for monomer C are shown in black as ball-and-stick. Residues Phe[62] and Trp[63] for a contacting symmetry molecule are shown in magenta. Figure was prepared with DINO.

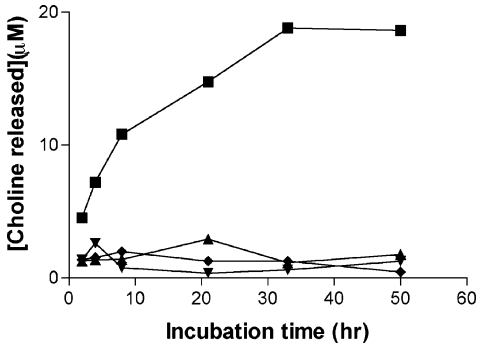

FIGURE 7: Time study of LPC production in the incubation mixture of GM2AP with PC. Reaction mixture contains: ■ 2.5 mg/mL GM2AP, 1 mM PC, 25 mM ammonium acetate pH 6.0. ▲ 1 mM PC, 2% β-octylglucoside, 25 mM ammonium acetate pH 6.0; ▼ 1 mM PC, 0.1% Triton X-100, 25 mM ammonium acetate pH 6.0; ◆ 1 mM PC, 25 mM ammonium acetate pH 6.0.

2−50 h period making use of the specificity properties of autotaxin, a lyso-phospholipase D enzyme that uses LPC, but not 18:1 PC as substrate (*31*). Lyso-PLD releases choline from LPC, converting it to lyso-phosphatidic acid. Figure 7 exhibits the time course of LPC production in terms of choline release. The reaction reaches a plateau at 36 h of incubation, which may indicate substrate depletion. Control experiments show that no LPC is produced (i) when GM2AP is absent in the reaction mixture and (ii) when PC is incubated in the presence of either 2% β-octylglucoside or 0.1% Triton X-100. This eliminates the possibility that LPC is produced by a general detergent effect. Both detergents do not affect the activity of autotaxin to hydrolyze LPC.

In the second assay, the release of free fatty acid products was measured directly in a sensitive fluorescence assay in which GM2AP was incubated with varying amounts of the fluorescent lipid PED6. PED6 serves as a sensitive probe to measure cleavage at the *sn*-2 glycerol ester bond. It is a modified phosphatidylethanolamine lipid with a palmitate substitution at the *sn*-1 position. Fluorescent moieties present at the *sn*-2 acyl tail and at the headgroup self-quench in the intact molecule. Figure 8a illustrates the kinetics of fatty acid release from the *sn*-2 acyl position as a function of substrate concentration (0.05−50 μM), showing typical sigmoidal behavior. Under these assay conditions, PED6 binds to GM2AP with a binding constant of 1.33 μM. As apparent

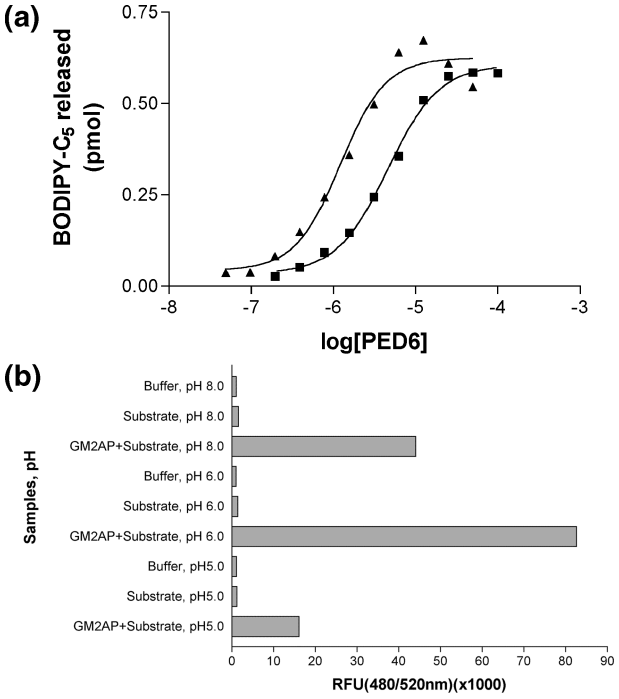

FIGURE 8: Analysis of the enzymatic activity of GM2AP using the PLA2 specific fluorescent lipid PED6. (a) Dependence of fluorescent intensity on PED6 concentration. Enzyme concentration is 0.01 mg/mL in 25 mM ammonium acetate buffer. ▲ reaction was carried out without $CaCl_2$; ■ reaction mixture contains 10 mM $CaCl_2$. Fluorescent measurements were made at 475 and 525 nm. (b) pH dependence of the hydrolysis of PED6. Each of the three conditions was tested with and without the addition of GM2AP. Values measured are relative fluorescence intensity.

from Figure 8b, the enzyme activity has a pH maximum of pH 6.0, contrasting with the pH 8 maxima observed for outer membrane phospholipase A of *E. coli* (OMPLA) (*32*, *33*) and many mammalian PLA2 enzymes (*34*, *35*). The enzyme efficiency with and without added calcium chloride can be deduced from Figure 8a. In contrast to other calcium-dependent PLA2 enzymes, it is interesting to note that the presence of calcium has no effect or even inhibits the esterase activity at higher substrate concentrations. In a control experiment, using the same conditions, cobra toxin exhibits no enzymatic activity at pH 6.0 in the absence of calcium. However, in the presence of calcium it shows a 20 times

weaker binding constant ($K_m = 20\mu M$) and a much greater turnover rate in comparison to GM2AP.

While the catalytic rate of the observed enzyme activity is low in comparison to members of the PLA2 enzyme family, it has unique properties showing a pH maximum at pH 6.0 and no increase in activity in the presence of calcium. The same observations were made for the glycosylated human form of GM2AP expressed in SF9 cells (data not shown), ruling out the possibility of a bacterial contaminant.

DISCUSSION

The structural data presented here, demonstrating that GM2AP can (i) bind multiple single chain phospholipids and fatty acids in its large binding pocket and (ii) hydrolytically modify phospholipids, suggests possibilities for yet unrecognized functions of GM2AP. For example, the combined effects of hydrolase activity coupled with lipid transport properties could provide a means of delivery of specific hydrolysis products to their target sites. Lyso-phospholipids and certain fatty acids are well-known to act as mediators in the complex area of cellular signaling and lipid metabolism. Hydrolase activity may also explain the inhibiting effect of GM2AP on PAF-induced disease processes, as these may simply be the result of enzymatic modification of PAF to nontoxic lyso-PAF.

The large lipophilic pocket, allowing low specificity binding of a heterogeneous mixture of lipids and their easy exchange, contrasts with the well-defined binding site architecture of other phospholipid binding proteins (*15*, *36*, *37*). For instance, lipid complexes of the lipid presenting mouse protein CD1d show the acyl chains bound in narrow channels (*37*). The ligands are thought to bind with high affinity (< micromolar), remaining bound until they can be released for further processing. Moreover, resident (endogenous) fatty acids that occupy the large pocket of GM2AP, as found in human and mouse apo-GM2AP and Y137S-PC, appear to have two functions. One is to maintain structural integrity of the protein fold, as also suggested for CD1b. The second one, as observed in our crystal structures, is its ability to attract and stabilize added lipid through nonpolar stacking interactions of their lipid tails.

Lipid bound inside the cleft region of the molecule, as observed in several crystal structures, suggests that this hydrophobic cleft may serve as a convenient channel to transfer lipid from the membrane to the hydrophobic pocket (*6*, *14*). To assess factors required for successful transfer, the importance of Tyr^{137} was considered because of its dual function. Replacement of its side chain by a serine hydroxyl group would (i) eliminate stacking with the phospholipid headgroup and (ii) destabilize the two alternate conformations of the mobile W131 loop (*6*). It was proposed that this loop acts as a flexible gate to the hydrophobic cleft, thus facilitating access of lipid to the binding pocket (*6*). Lipid entry would be permitted when it is flipped out exposing Trp^{131}, and blocked when it is turned in with the indole ring of Trp^{131} roughly taking up the position of the phospholipid headgroup. The conformational state of this loop is not a function of pH, as both conformations are observed in the low and high pH structures.

Replacement of Tyr^{137} by serine not only resulted in formation of a new crystal form but also affected mobility and structural integrity of the W131 loop (Figure 5b). In addition, it caused closure of the cleft as a result of an inward shift of the disordered strand Asp^{125}-Leu^{128}. The absence of lipid inside the binding pocket and near Tyr^{71} further supports the view that the cleft acts as a transfer channel. We infer from analysis of this mutant structure that both the open and the closed conformations of the cleft are essential for lipid entry and transfer. The tyrosyl side chain of Tyr^{137} is crucial for structural integrity of the open conformation necessary to allow lipid entry.

Hydrolytic activity associated with GM2AP was suggested previously based on structure analysis of GM2AP−PAF (*14*). This structure revealed binding of intact PAF in the hydrophobic cleft of all three monomers in the asymmetric unit and lyso-PAF in binding site II. Although both PAF and PC are susceptible to auto-oxidation, it is unlikely that LPC and lyso-PAF would be produced at high enough concentrations for binding. As verified by mass spectrometry analysis, neither lyso-PAF nor LPC could be detected among a series of breakdown products in samples of both lipids stored at room temperature in aqueous solution for several days. Identification of glycero-3-phosphocholine in two monomers of GM2AP3-PC suggests, in addition, that cleavage had occurred to a lesser extent at the *sn*-1 ester bond of PC. Thus, the enzyme activity resembles that of the well-known enzymes PLA2 and PLA1. The phospholipase A enzymes encompass a large structurally diverse family of proteins found both extracellularly and intracellularly in the cytosol (*34*, *35*). Their biological significance lies to a large extent in their ability to generate hydrolysis products that can act as second messengers in cellular signaling processes. These enzymes vary in their calcium and pH dependence and in the structural features of their active sites (Ser-His-Asp or Ser-Arg-Asp). For many it has been shown that they act at the lipid/water interface and require dimerization (*38*). A similar mechanism could apply to GM2AP. However, we have as yet not been able to identify the hydrolytic site on the protein surface. Assuming that the putative active site contains a His residue, the two histidines in the molecule (His^{79} and His^{106}) are exposed on the surface near the N-terminal end of the single α-helix. However, there is no clear evidence for a catalytic triad as required for successful hydrolysis. Several Asp residues in the vicinity can only interact with the imidazole rings through water mediated contacts. It is possible that other factors, such as dimerization, are required for successful catalysis.

CONCLUSIONS

We have shown that incubation of GM2AP with 18:1 PC results in a heterogeneous mixture of stable protein lipid complexes. Three different crystal forms were analyzed, containing one, two, and three monomers per asymmetric unit. Each structure shows distinct structural features with respect to lipid binding and flexibility of loop regions. The available nonprotein electron density inside the apolar pocket is insufficient to suggest that intact PC is bound, although it could easily be spatially accommodated. It was modeled as LPC, PCH, and OLA thought to constitute deacylation products of PC, and other smaller fatty acids. The presence of LPC in the incubation mixture with PC was verified by mass spectrometry and by an enzymatic assay that uses LPC as substrate. Direct evidence for enzymatic activity was

further obtained from a fluorescence assay that uses a PLA2-specific fluorescent lipid. The hydrolase activity was found to have a pH maximum at pH 6.0 and does not require calcium. The presence of calcium lowers the binding constant and causes weak inhibition.

In agreement with earlier studies (*14*), binding locations I (cleft area) and II (inside pocket) are occupied by LPC and/or fatty acids in the "open" structures. The "closed" structures of GM2AP2-PC and GM2AP3-PC (monomer C) exhibit LPC binding only in site II near Ser^{141} and fatty acid binding near Tyr^{71} and Phe^{121} (Figure 3b). Although lipid binding was found not to be identical in all complexes, taken together the positions of the alkyl chains coincide to a large extent and site II is preferentially occupied. Short chain fatty acids may represent resident fatty acids that become ordered through nonpolar stacking interactions with bound incoming ligand. Supporting evidence for the putative functional role of the hydrophobic cleft as lipid transfer channel was obtained from the structure of mutant Y137S. While its overall structure is similar to that of GM2AP2-PC, absence of lipid inside the pocket suggests that the conformational change in the W131 mobile loop, caused by the mutation, may lock the cleft into a permanently closed conformation, blocking lipid entry.

ACKNOWLEDGMENT

We thank the staff of beamlines IMCA-CAT and SERCAT (APS) for their assistance with data collection. We are also grateful to Dr. Kevin Lynch for helpful discussions, to Dr. Su-Chen Li (Tulane University) for supplying protein samples of mouse GM2AP for crystallization, and to Dr. D. Abraham for providing data collection facilities (R-axis image plate detector) to determine its structure.

REFERENCES

1. Fürst, W., and Sandhoff, K. (1992) Activator proteins and topology of lysosomal sphingolipid catabolism, *Biochim. Biophys. Acta 1126*, 1−16.
2. Li, Y.-T., and Li, S.-C. (1984) Activator proteins related to the hydrolysis of Glycosphingolipids catalyzed by lysosomal glycosidases, in *Lysosomes in Biology and Pathology* (Dingle, J. T., Dean, R. T., Sly, W., Eds.) pp 99−117, Elsevier Science Publishers, Amsterdam.
3. Wright, C. S., Li, S.-C., and Rastinejad, F. (2000) Crystal structure of human GM2-activator Protein with a novel β-cup topology, *J. Mol. Biol. 304*, 411−422.
4. Ahn, V. E., Faull, K. F., Whitelegge, J. P., Fluharty, A. L., and Prive, G. G. (2002) Crystal structure of saposin B reveals a dimeric shell for lipid binding, *Proc. Nat. Acad. Sci. U.S.A. 100*, 38−48.
5. Conzelmann, E., Burg, J., Stephan, G., and Sandhoff, K. (1982) Complexing of glycolipids and their transfer between membranes by the activator protein for degradation of lysosomal ganglioside GM2, *Eur. J. Biochem. 123*, 455−464.
6. Wright, C. S., Zhao, Q., and Rastinejad, F. (2003) Structural analysis of Lipid complexes of the GM2-activator protein, *J. Mol. Biol. 331*, 951−964.
7. Mahuran, D. J. (1998) The GM2 activator protein, its roles as a co-factor in GM2 hydrolysis and as a general glycolipid transport protein, *Biochim. Biophys. Acta 1393*, 1−18.
8. Rigat, B., Wang, W., Leung, A., and Mahuran, D. J. (1997) Two mechanisms for the recapture of extracellular GM2 activator protein: Evidence for a major secretory form of the protein, *Biochemistry 36*, 8325−8331.
9. Zhou, D., Cantu, C., III, Sagiv, Y., Schrantz, N., Kulkarni, A. B., Qi, X., Mahuran, D. J., Morales, C. R., Grabowski, G. A., Benlagha, K., Savage, P., Bendelac, A., and Teyton, L. (2004) Editing of CD1d-bound lipid antigens by endosomal lipid transfer proteins, *Science 303*, 523−527.
10. Gadola, S. D., Zaccai, N. R., Harlos, K., Shepherd, D., Castro-Palomino, J. C., Ritter, G., Schmidt, R., R., Jones, E. Y., and Cerundolo, V. (2002) Structure of human CD1b with bound ligands at 2.3 Å, a maze for alkyl chains, *Nat. Immun. 3*, 721−726.
11. Rigat, B., Reynaud, D., Smiljanic-Georgijev, N., and Mahuran, D. (1999) The GM2 activator protein, a novel inhibitor of platelet-activating factor, *Biochem. Biophys. Res. Commun. 258*, 256−259.
12. Nakamura, S., Akisue, T., Jinnai, H., Hitomi, T., Sarkar, S., Miwa, N., Okada, T., Yoshida, K., Kuroda, S., Kikkawa, U., and Nishizuka, Y. (1998) Requirement of GM2 ganglioside activator for phospholipase D activation, *Proc. Natl. Acad. Sci. U.S.A. 95*, 12249−12253.
13. Zarkar, S, Miwa, N., Kominami, H., Igarashi, N., Hayashi, S., Okada, T., Jahangeer, S., and Nakamura, S. (2001) Regulation of mammalian phospholipase D2: interaction with and stimulation of GM2 activator, *Biochem. J. 359*, 599−604.
14. Wright, C. S., Mi, L.-Z., and Rastinejad, F. (2004) Evidence for lipid packaging in the crystal structure of the GM2-activator complex with platelet activating factor, *J. Mol. Biol. 342*, 585−592.
15. Roderick, S. L., Chan, W. W., Agate, D. S., Olsen, L. R., Vetting, M. W., Rajashankar, K. R., and Cohen, D. E. (2002) Structure of human phosphatidylcholine transfer protein in complex with its ligand, *Nat. Struct. Biol. 9*, 507−511.
16. Wendeler, M., Hoernschemeyer, J., Hoffmann, D., Kolter, T., Schwarzmann, G., and Sandhoff, K. (2004) Photoaffinity labelling of the human GM2-activator protein. Mechanistic insight into ganglioside GM2 degradation, *Eur. J. Biochem. 271*, 614−627.
17. Yuziuk, J. A., Bertoni, C., Beccari, T., Orlacchio, A., Wu, Y.-Y., Li, S.-C., and Li, Y.-T (1998) Specificity of mouse GM2 activator protein and beta-*N*-acetyl-hexosaminidase A and B, *J. Biol. Chem. 273*, 66−72.
18. Bertoni, C., Li, Y.-T., and Li, S.-C. (1999) Catabolism of Asialo-GM2 in man and mouse, *J. Biol. Chem. 274*, 28612−28618.
19. Wright, C. S., and Li, S.-C. (1997) Crystallization and preliminary X-ray characterization of GM2-activator protein, *Acta Crystallogr. Sect. D 53*, 211−212.
20. Otwinowski, Z., and Minor, W.(1997) Processing of X-ray diffraction data collected in oscillation mode, *Methods Enzymol. 276*, 307−326.
21. Collaborative Computational Project, Number 4 (1994). The CCP4 Suite: programs for protein crystallography, *Acta Crystallogr. Sect. D 50*, 760−763.
22. Vagin, A., and Teplyakov, A.(2000) An approach to multi-copy search in molecular replacement, *Acta Crystallogr. Sect. D 56*, 1622−1624.
23. Jones, T. A., and Kjeldgaard, M. (1993) O Version 5.9, The Manual, Uppsala University, Uppsala, Sweden.
24. Brünger, A. T., Adams, P. D., Clore, G. M., Delano, W. L., Gross, P., Grosse- Kunstleve, R. W. et al. (1998) Crystallographic and NMR system − a new software suite for macromolecular structure determination, *Acta Crystallogr. D54*, 905−921.
25. Kleywegt, G. T., and Jones, T. A. (1998) Databases in protein crystallography, *Acta Crystallogr. Sect. D 54*, 119−1131.
26. Van Meeteren, L. A., Frederiks, F., Giepmans, B. N. G., Pedrosa, M. F. F., Billlington, S. J., Jost, B. H., Tambourgi, D. V., and Moolenaar, W. H. (2004). Spider and bacterial sphingomyelinases D target cellular lysophosphatidic acid receptors by hydrolyzing lysophophatidylcholine, *J. Biol. Chem. 279*, 10833−10836.
27. Umezu-Goto, M., Kishi, Y., Taira, A., Hama, K., Dohmae, N., Takia, K., Yamori, T., Mills, G. B., Inoue, K., Aoki, J., and Arai, H. (2002) Autotoxin has lyso-phospholipase D activity leading to tumor cell growth and motility by lyso-phosphatidic acid production, *J. Cell. Biol. 158*, 197−199.
28. Göpfert, M., Siedler, F., Siess, W., and Sellmayer, A. (2005) Structural identification of oxidized acyl-phosphatidylcholines that induce platelet activation, *J. Vasc. Res. 42*, 120−132.
29. Thompson, J., Ory, J., Reese-Wagoner, A., and Banaszak, L. J. (1999) The liver fatty acid binding protein − comparison of cavity properties of intracellular lipid-binding proteins, *Mol. Cell. Biochem. 192*, 9−16.
30. Thompson, J. R., and Banaszak, L. J. (2002) Lipid−protein interactions in Lipovitellin, *Biochemistry 41*, 9398−9409.
31. Tokumura, A., Majima, E., Kariya, Y., Tominaga, K., Kogure, K., Yasuda, K., and Fukuzawa, K. (2002) Identification of human

plasma lysophospholipase D, a lysophosphatidic acid-producing enzyme, as autotaxin, a multifunctional phosphodiesterase, *J. Biol. Chem. 277*, 39436−39442.
32. Dekker, N., Merck, K., Tommassen, J., and Verheij, M. (1995) In vitro folding of *Escherichia coli* out-membrane phospholipase A, *Eur. J. Biochem. 232*, 214−219.
33. Snijder, H. J., Kingma. R. L., Kalk, K. H., Dekker, N., Egmond, M. R., and Dijkstra, B. W. (2001) Structural investigation of calcium binding and its role in activity and activation of outer membrane phospholipase A from *Escherichia coli*, *J. Mol. Biol. 309*, 477−489.
34. Dennis, E. A. (1994) Diversity of group types, regulation, and function of Phospholipase A2, *J. Biol. Chem. 269*, 13057−13060.
35. Dennis, E. A. (1997) The growing phospholipase A2 superfamily of signal transduction enzymes, *Trends Biol. Sci. 22*, 1−2.
36. Beamer, L. J., Carroll, S. F., and Eisenberg, D. (1997) Crystal structure of human BPI and two bound phospholipids at 2.4 angstrom resolution, *Science 276*, 1861−1864.
37. Batuwangala, T., Shepherd, D., Gadola, S. D., Gibson, K. J. C., Zaccai, N. R., Fersht, A. R., Besra, G. S., Cerundolo, V., and Jones E. Y. (2004) The crystal structure of human CD1b with a bound bacterial glycolipid, *J. Immunol. 172*, 2382−2388.
38. Pan, Y. H., Yu, B.-Z., Berg, O. G., Jain, M. K., and Bahnson, B. J. (2002) Crystal structure of phospholipase A2 complex with the hydrolysis products of platelet activating factor: Equilibrium binding of fatty acid and lysophospholipid-ether at the active site may be mutually exclusive, *Biochemistry 41*, 14790−14800.

BI050668W